JOURNAL OF MATERIALS SCIENCE 24 (1989) 4144–4151

# Microstructure and mechanical properties of RB-SiC/$MoSi_2$ composite

C. B. LIM, T. YANO, T. ISEKI
*Research Laboratory for Nuclear Reactors, Tokyo Institute of Technology, Ohokayama, Meguro-ku, Tokyo 152, Japan*

Microstructure, high temperature strength and oxidation behaviour of reaction bonded silicon carbide, RB-SiC/17 wt% $MoSi_2$ composite prepared by infiltrating a porous RB-SiC bulk (after removal of free silicon) with molten $MoSi_2$ were investigated. There was good bonding between the SiC and $MoSi_2$ particle, without a significant reaction zone and microcracking caused by the thermal mismatch stresses. A thin ($\sim$2 nm) layer, however, was observed at the SiC/$MoSi_2$ interfaces. At room temperature, the composite exhibited a bending strength of 410 MPa, which is $\sim$20% loss in comparison to that of RB-SiC alone (containing $\sim$10 wt% free silicon). However, the composite strength increased to a maximum of 590 MPa in the temperature range 1100 and 1200° C and dropped to 460 MPa between 1200 to 1400° C, after which the strength remained constant. The passive oxidation of the composite in dry air in the temperature range 1300 to 1400° C was found to follow the parabolic rate law with the formation of a protective layer of cristobalite on the surface.

## 1. Introduction

Reaction bonded silicon carbide (RB-SiC), because of its adequate mechanical strength and good oxidation resistance, is an obvious candidate for ceramic components in gas turbine engines, heat exchangers, and wear resistant seals. It can be fabricated into fully dense complex shapes without shrinkage during reaction bonding. From these characteristics, RB-SiC has an advantage over other structural ceramics and has great potential as a high performance ceramic. The RB-SiC is typically fabricated by infiltrating a compacted body of SiC filler and graphite with molten silicon. The molten silicon rises through the porous compact by capillary action, converting the graphite to "new" SiC which bonds the original SiC together. These process and mechanical properties have been fully described elsewhere [1–4]. The major problem impeding the use of RB-SiC, as a high temperature structural material, is its mechanical property in that it's strength drops off rapidly at the melting temperature of silicon (1410° C) [1].

In order to improve the problem, this paper represents a new approach in producing a RB-SiC/molybdenum disilicide ($MoSi_2$) composite (without free silicon) that is fabricated by a molten $MoSi_2$ re-infiltration type of operation into a nearly final shape with little if any dimensional changes. It is possible to re-infiltrate molten $MoSi_2$ into porous RB-SiC bulk after nearly-complete removal of free silicion, because the free silicon is linked to form a continuous network between the sturdy SiC skeleton within the RB-SiC bulk. $MoSi_2$ was selected because it is a very attractive intermetallic compound with a much higher melting point of 2000 $\pm$ 20° C. It has many of the physical characteristics of metals, notably adequate high temperature strength and good thermal shock resistance [5]; its oxidation resistance at high temperatures is excellent, clearly the best of the silicides and nearly as good as SiC [6, 7].

Past investigations have revealed mechanical properties in some types of SiC/$MoSi_2$ which were fabricated by infiltrating porous SiC body with molten $MoSi_2$ and silicon at 2100° C [8, 9], or at 1500° C starting with an $MoSi_2$ suspension on the internal and external surfaces of the porous SiC body [10]. A similar approach has recently been developed which describes the toughening and strengthening of a $MoSi_2$ matrix by the addition of SiC whiskers [11, 12]. Nevertheless, high temperature mechanical properties and microstructural features in much greater detail have not been described to understand RB-SiC/$MoSi_2$ composite.

The objectives of this paper are to demonstrate how a RB-SiC/$MoSi_2$ composite is fabricated and to investigate the high temperature strength and oxidation resistance of the composite. Particular emphasis is also placed on the microstructural features, such as interfacial condition and fracture mode, which has been undertaken employing scanning electron microscopy (SEM) and transmission electron microscopy (TEM).

## 2. Experimental procedure

### 2.1. Measurement of contact angles of $MoSi_2$ on pressureless-sintered SiC

The $MoSi_2$ bulk was prepared by melting a commercial powder ($MoSi_2$-F from Japan New Metal Co. Ltd, Õsaka, grain size 2.1 $\mu$m) in vacuum (0.65 Pa) for 30 min at 2050° C. A cubic specimen was cut from the ingot and beveled at the base to ensure a uniform advancing contact angle on melting. A pressureless



0022–2461/89 $03.00 + .12 

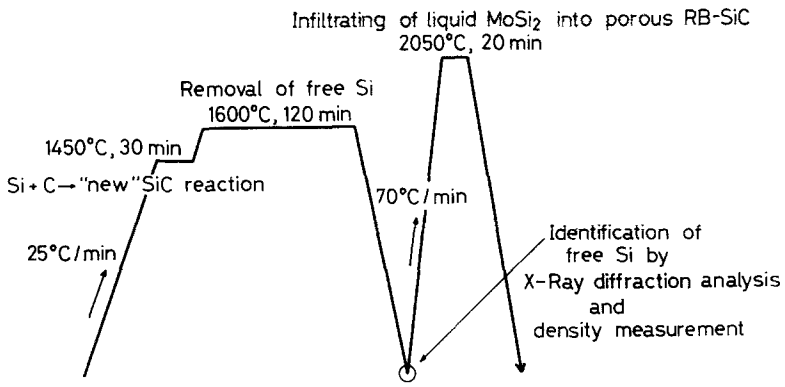


*Figure 1* Schematic temperature–time schedule for the fabrication of a RB-SiC/$MoSi_2$ composite.

sintered (PLS) SiC (from Kyocera Co. Ltd, Kyoto) with densities of 3.10 g cm$^{-3}$ was cut into plate of 20 mm × 10 mm × 4 mm and polished to a ~1 μm diamond paste finish.

Contact angles were measured by the sessile drop method. The sample was heated to a temperature near the melting point of $MoSi_2$ while a vacuum of 0.65 Pa was held to outgas the system. After the $MoSi_2$ melted, photographs of the plate and drop combination were taken at several temperatures. Contact angles were measured directly from the photographs with a protractor.

### 2.2. Preparation of RB-SiC/$MoSi_2$ composite

RB-SiC was prepared by the method previously described [3, 4]. The raw materials were α-SiC filler (GC 2000 from Fujimi Kenmazai Kogyo Co. Ltd, Nagoya, grain size 7.9 μm) and carbon black (Diablack I from Mitsubishi Chemical Industries Ltd, Tokyo, grain size 0.02 μm). Powders of α-SiC and carbon were mixed in a ratio of 2 : 1, then uniaxially pressed into plates of about 26 mm × 26 mm × 6 mm at 25 MPa in a graphite die. The plates were next isostatically pressed at 260 MPa in thin-walled rubber.

Schematic temperature–time schedule for the fabrication of a RB-SiC/$MoSi_2$ composite is shown in Fig. 1. All the plates were fired in graphite crucible inside a graphite resistance furnace under vacuum (0.65 Pa). The bulk density of porous RB-SiC after the removal of free silicon was ~2.85 g cm$^{-3}$, giving a porosity of ~11%. The $MoSi_2$ powder (grain size 2.1 μm) was used for re-infiltration into the porous RB-SiC bulk. X-ray diffraction (XRD) analysis confirmed the powder to be pure $MoSi_2$ with no other crystalline species detected, and spectrochemical analysis revealed 0.12 wt % iron and 0.05 wt % carbon as the major impurities. The bulk density of the resulting RB-SiC/$MoSi_2$ composite was measured by Archimedes immersion technique using water, after surface-polishing to ~1 μm.

### 2.3. Microstructural observations

The phase identification was performed by XRD analysis. The polished surface was examined by optical microscopy and SEM after thermal etching for 10 min at 1500° C under vacuum. The microstructural features of the fractured surfaces and thinned specimens were examined by SEM and TEM, respectively.

### 2.4. Measurement of thermal expansion coefficient, electrical resistance, high temperature strength and oxidation resistance

The composite material was sectioned into a bar 24 mm long by 4 mm wide by 2 mm thick and polished to ~1 μm in the longitudinal direction with section planes parallel to the infiltrating direction of molten $MoSi_2$.

The thermal expansion coefficient was measured using a differential dilatometer, from room temperature to 1000° C in argon (1 atm).

Electrical resistance was measured using a four-contact circuit in which a current of 1 mA was passed through the sample and the voltage variation between a pair of probes 1 cm apart was measured.

For high temperature bending strength testing, the two edges on the tensile surface of the specimens were rounded, and a four-point bending test with an inner span of 10 mm and outer span of 20 mm, and a cross-head speed of 0.5 mm min$^{-1}$ was carried out with elevating temperature under vacuum (1.3 × 10$^{-2}$ Pa).

For the oxidation resistance measurement, the weight gain or weight loss per unit area of the samples was determined when oxidized at 1300° C for 200 h and 1400° C for 100 h in dry air. An SEM observation and XRD analysis of the oxidized surface of the samples were also carried out.

## 3. Results and discussion

### 3.1. Wetting of SiC by $MoSi_2$

The PLS-SiC was wet by $MoSi_2$ at 1970° C, just below its melting point (2000 ± 20° C), with a contact angle of 42° (Fig. 2). In the present experiment, the decomposition of $MoSi_2$ did not occur up to 2050° C, but it was sensitive at > 2100° C (primarily on the PLS-SiC bulk surface). There was, as shown in Fig. 2, no presence of a reaction at the SiC/$MoSi_2$ interface (refer to Figs 4, 5 and section 3.2).

Because the SiC is thus easily wet by the $MoSi_2$, the molten $MoSi_2$ can rise quite rapidly through the porous RB-SiC bulk.

### 3.2. Microstructural observations

The bulk density of the resulting composite was ~3.39 g cm$^{-3}$, giving a calculated $MoSi_2$ content of ~17 wt %, and suggesting that there were ~2% pore with no free silicon within the specimens (see Fig. 11 (IIa)).

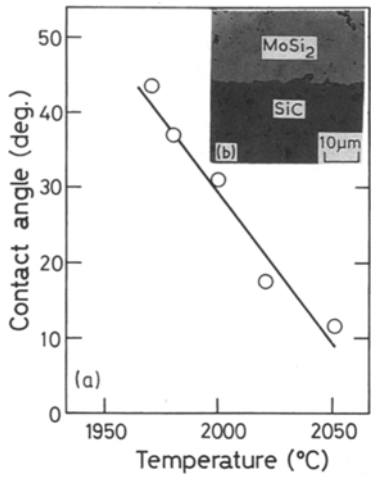


*Figure 2* (a) Effect of temperature on contact angle of $MoSi_2$ on PLS-SiC. (b) Optical micrograph taken at $MoSi_2$/SiC interface shows no chemical reaction zone.

Figure 3 reveals a dense microstructure of the composite, in which the $MoSi_2$ almost fills up the pores formed by the removal of free silicon. The TEM micrographs and bulk XRD results given in Figs 4, 5 and 11 (IIa), which show that crystallographic phase of $MoSi_2$ and SiC are tetragonal (t) and α, respectively. This agrees well with the fact that t-$MoSi_2$ and α-SiC are more stable than the other polytype at $> 800°$ C [13] and at $> 1800°$ C [2], respectively. During re-infiltrating of liquid $MoSi_2$ into the porous RB-SiC, significant grain growth of SiC did not occur. The grain growth of α-SiC crystals, was noted in hot-pressed materials heat treated at 2200° C [14].

At room temperature, $MoSi_2$ behaves in a brittle failure, but at high temperature, some plastic deformation takes place. This is explained well by Fig. 4 exhibiting sufficient dislocation in the $MoSi_2$ domain. On the other hand, in the SiC domain, strain contrasts were observed with the contrasts due to stacking faults.

Thermodynamic calculations indicate that SiC and $MoSi_2$ should not react at 1600 to 1700° C temperatures [11]. The possibility exists that $MoSi_2$ at the SiC particle surfaces may have undergone a chemical reaction ($3SiC + 4Mo \rightleftharpoons Mo_4CSi_3 + 2C$) [15] as a result of the high temperature re-infiltration conditions (2050° C). However, Fig. 5 reveals the absence of a reaction zone at the SiC/$MoSi_2$ interface. It is speculated that the reaction zone, if present, is related to the iron and carbon impurities present in the $MoSi_2$. The interfacial layer shown in Fig. 5 seems to contain amorphous material. Ness and Page [2] reported that SiC–SiC grain boundaries, SiC–SiC epitaxial boundaries and SiC–Si interfaces comprise a thin ($\sim 1$ nm) layer of amorphous SiC. It is not obvious whether this interfacial layer was formed during reaction-bonding or during $MoSi_2$ re-infiltrating, in the present study.

As can be clearly seen in the above microstructural observation results, there was good bonding between the $MoSi_2$ and SiC, without microcrack being formed during cooling down from its fabrication temperature. The microcracking possibility in this system, is discussed in Section 3.4.

## 3.3. Physical and mechanical properties

### *3.3.1. Thermal expansion coefficient and electrical resistance*

The considerable difference in physical properties, such as thermal expansion coefficient and electrical resistance was not found between the RB-SiC alone (containing 10 wt % free silicon) and the RB-SiC/17 wt % $MoSi_2$ composite. It is considered that these causes are related to the pores present in the RB-SiC/$MoSi_2$ composite. The results are summarized in Table I.

### *3.3.2. High temperature bending strength and fracture mode*

At room temperature, the RB-SiC/$MoSi_2$ composite exhibited a bending strength of 410 MPa, which is low in comparison to that of RB-SiC alone (520 MPa) (Fig. 6). However, the composite strength increased to a maximum (590 MPa) in temperature range 1100 to 1200° C and dropped to 460 MPa between 1200 to 1400° C, after which the strength remained constant. On the other hand, the strength of RB-SiC alone decreased to 240 MPa at the temperature above 1400° C because of the loss of strength of silicon as the temperature approaches the melting point of 1410° C.

Since overall the $MoSi_2$ appeared to be strongly bonded to the SiC, the debonding at the $MoSi_2$–SiC interface would not be expected at room temperature (Fig. 7a). There was, however, significant evidence of the debonding at the $MoSi_2$–SiC interface with

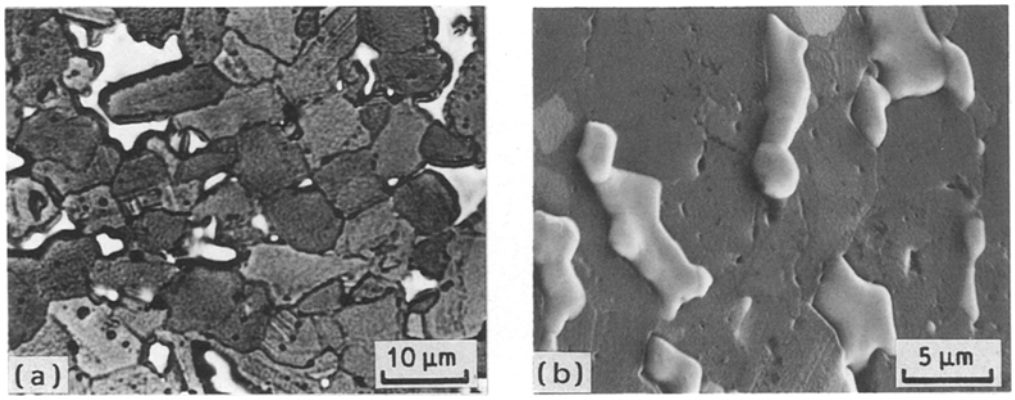


*Figure 3* (a) Optical micrograph and (b) SEM micrograph of polished surface of RB-SiC/$MoSi_2$ composite prepared by thermal etching at 1500° C for 10 min, exhibiting dense microstructure without grain growth of SiC. Dark part is SiC, and light (white) part is $MoSi_2$.

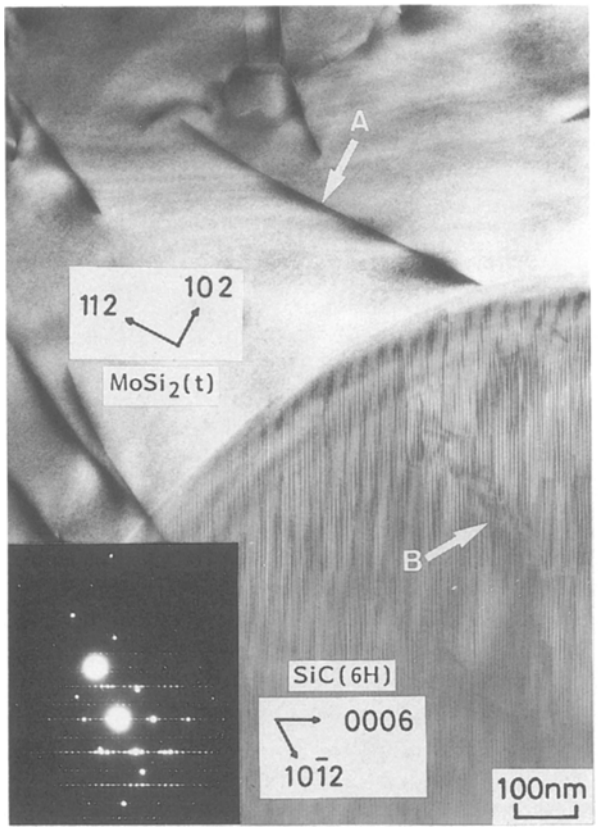


*Figure 4* TEM micrograph showing grain boundary (interface) between $MoSi_2$ and α-SiC; diffraction pattern (lower left) taken at boundary indicates orientation relation of grains. Straight lines (arrowed A) in $MoSi_2$ represent dislocation and dark areas (arrowed B) in α-SiC represent strain contrasts.

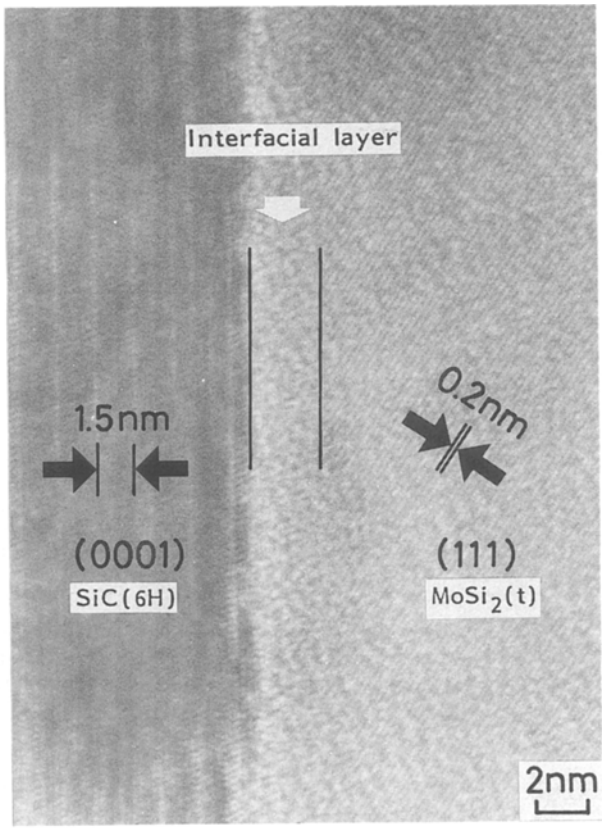


*Figure 5* TEM micrograph of $MoSi_2$/SiC interface showing respective lattice fringe image and interfacial layer width to be determined as ~2 nm.

transgranular fracture in the SiC at high temperature (Fig. 7c). In addition, during testing of the specimens, cracks appeared adjacent to the $MoSi_2$ particle because of the applied stresses at room temperature (Fig. 7a), but there were no cracks at high temperature (Fig. 7c).

In the composite systems, it is found that the important strength-controlling factors include: (a) thermal expansion coefficients and the elastic properties of the two phases; (b) the volume fraction and average particle size of the second-phase dispersion [16, 17]. Lange [18] postulated that a change in microstructure of the composite system may effect one of the strength-controlling factors more than the others. Relation equations (theory) concerning the stress system around particles in an isotropic medium due to a thermal expansion mismatch, as a function of volume fraction and particle size of the second phase dispersion, are therefore well established [16–20]. In general, these equations hold for the case of the composite system with second phase distributed as discrete particles within a matrix phase, but it is doubtful whether they represent a satisfactory approximation for the case of the RB-SiC/$MoSi_2$ composite with second phase ($MoSi_2$) distributed as a continuous network within the SiC material. Consequently, only the effect due to thermal expansion mismatch between $MoSi_2$ and SiC will be assessed in this study.

The thermal expansion mismatch between $MoSi_2$ and SiC (i.e., $MoSi_2$: $8.1 \times 10^{-6}$ to $8.8 \times 10^{-6}\,°C^{-1}$ against SiC: $4.3 \times 10^{-6}$ to $5.4 \times 10^{-6}\,°C^{-1}$) causes residual stresses within and around the larger $MoSi_2$ crystal when the composite cools down from its fabrication temperature, as shown in Fig. 8. The residual tensile stress around $MoSi_2$ in the infiltration path is negligible because the width of the path is very narrow. It is then expected that the radial tensile stress can induce tangential microcracks in the SiC around each $MoSi_2$ particle. However, no microcrack formation during cooling was recognized for the SiC and $MoSi_2$ particle, as illustrated in Section 3.2, but a certain amount of strain was only observed in the SiC. According to Ness and Page [2], this strain in RB-SiC

TABLE I Room-temperature physical properties

| Description | Porosity | Thermal expansion coefficient ($°C^{-1}$) | Electrical resistance (Ω.cm) |
|---|---|---|---|
| RB-SiC alone (containing 10 wt % free Si) | ~0 | $4.3 \times 10^{-6}$ | $1.7 \times 10^{-1}$ |
| RB-SiC + 17 wt % $MoSi_2$ | ~2 | $4.2 \times 10^{-6}$ | $3.1 \times 10^{-2}$ |

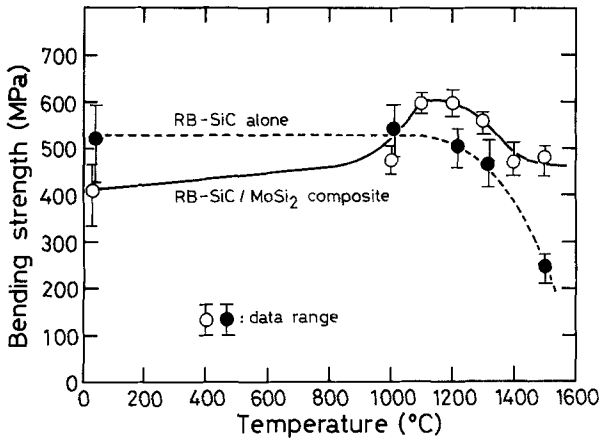


*Figure 6* Strength variations of RB-SiC/$MoSi_2$ composite and RB-SiC alone with temperature. Each point represents at least three individual tests.

alone may be due to the residual stress caused by the thermal expansion mismatch. The room-temperature strength reduction of the composite shown in Fig. 6 may be, therefore, attributed to the residual tensile stress. Recently, Carroll and Tressler [21] investigating the static load-dependent strength of RB-SiC, reported that the strength decrease is related to the residual tensile stress alone. The cracks shown in Fig. 7a may be due to the overlap applied stress to areas with high level of concentrated residual stresses including residual tensile stresses. In the RB-SiC/$MoSi_2$ composite system, the strength decrease by the stress concentration due to elastic moduli differences and pores do not appear because (1) the elastic moduli of SiC and $MoSi_2$ are nearly the same (SiC: 420 GPa, $MoSi_2$: 410 GPa), and (2) the size of the pores is much smaller than that of the SiC and $MoSi_2$ particle, and are located at the centre of larger $MoSi_2$ particle (refer to Fig. 10a); effect of pores on strength has been explained by Davidge [17].

It is thought that the possible reasons for the increase in fracture strength of the composite at high temperature are (1) lowering the thermal mismatch stresses compared with that at room temperature, and (2) the brittle-to-ductile transition of $MoSi_2$, at $< 1000°$ C. Claussen *et al.* [22] reported that at high temperature, the thermal mismatch stresses in the composite are much lower than at room temperature and the interfacial layer has softened such that some modulus load transfer has become operative. Hillig *et al.* [23] reported that the increase in the transverse strength in the Si/SiC composite (SILCOMP, General Electric Co., Schenectady, New York) between 900 and 1300° C is attributed to the ability of the silicon

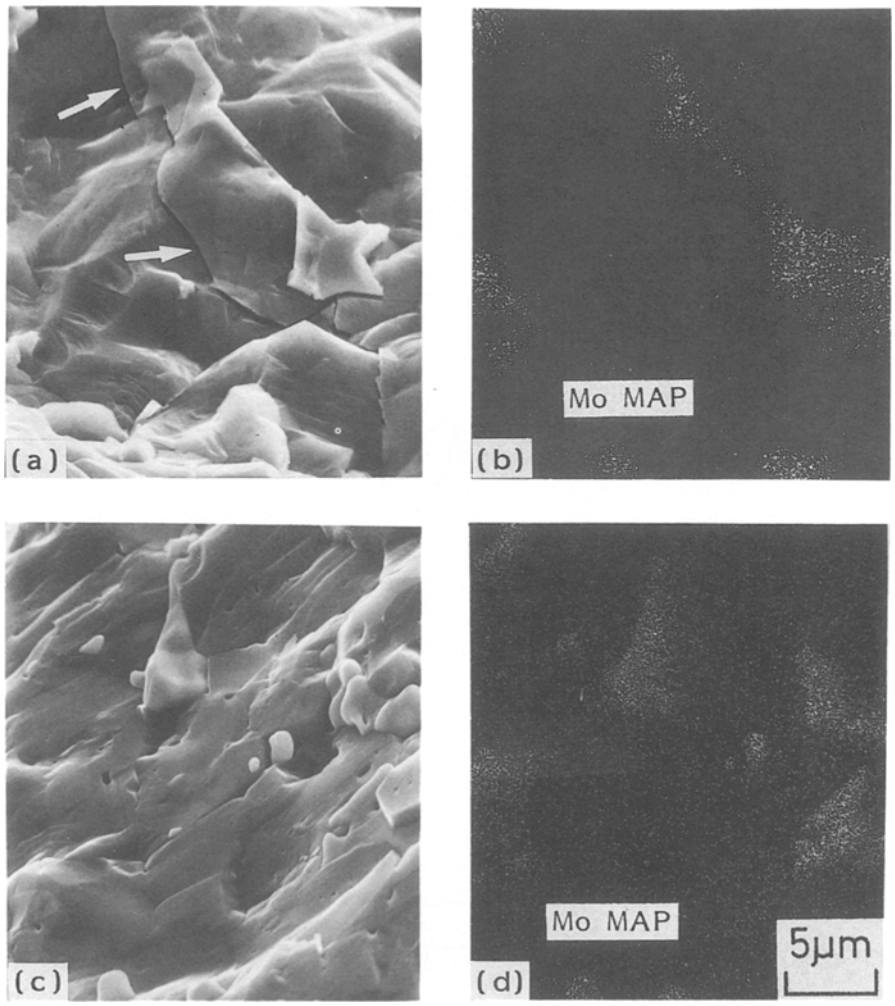


*Figure 7* SEM micrographs of RB-SiC/$MoSi_2$ composite fractured (a, b) at room temperature and (c, d) at 1500° C. At room temperature, transgranular cracks (arrows) domain caused by the applied stress occasionally appeared in the SiC domain adjacent to the $MoSi_2$ crystal. At 1500° C, there was significant evidence of debonding at $MoSi_2$–SiC interface.

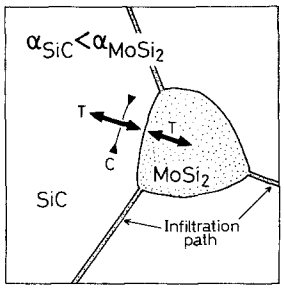


*Figure 8* Schematic of effects of localized stresses caused by thermal expansion mismatch. $\alpha$: thermal expansion coefficient. T and C represent radial tensile stresses and tangential compressive stress, respectively.

to deform plastically without losing too much strength, thus alleviating the effect of stress raisers. Consequently, at least as $> 1000°$ C, the cracking shown in Fig. 7a is not observed, which is probably due to tensile stress reduction. The debonding at the $MoSi_2$–SiC interface shown in Fig. 7c, has become more effective due to ductility of $MoSi_2$.

### 3.3.3. Oxidation behaviour

The passive oxidation of the RB-SiC/17 wt % $MoSi_2$ composite in dry air under 1 atm pressure at 1300 and 1400° C followed a parabolic behaviour, as shown in Fig. 9a and b where the square of the weight gain is plotted as a function of exposure time. The parabolic rate constants ($k_p$) for the oxidation of the composite were $3 \times 10^{-9}$ g$^2$ cm$^{-4}$ h$^{-1}$ at 1300° C and $5.1 \times 10^{-9}$ g$^2$ cm$^{-4}$ h$^{-1}$ at 1400° C.

It is well known that Si, SiC and $MoSi_2$ are all thermodynamically unstable in air at high temperature, but the degree of oxidation is commonly limited by the formation of a protective silica layer [24–27]. The so called "passive oxidation" is characterized by the formation of the protective silica layer according to:

$$Si(s) + O_2(g) \rightarrow SiO_2(s) \quad (1)$$

$$SiC(s) + 3/2O_2(g) \rightarrow SiO_2(s) + CO(g) \quad (2)$$

$$MoSi_2(s) + 7/2O_2(g) \rightarrow MoO_3(s) + 2SiO_2(s) \quad (3)$$

$$5MoSi_2(s) + 7O_2(g) \rightarrow Mo_5Si_3(s) + 7SiO_2(s) \quad (4)$$

The reaction of Si, SiC and $MoSi_2$ with $O_2$ occurs at the Si–$SiO_2$, SiC–$SiO_2$ and $MoSi_2$–$SiO_2$ interface, respectively. For the oxidation behaviour of $MoSi_2$, in the initial stages, the oxide layer is formed according to the Reaction 3. However, preferential oxidation of silicon, occurring according to Reaction 4, results in the formation of $Mo_5Si_3$. The growth of silica layer in the $MoSi_2$ system is detected by the rate of diffusion of silicon from the $MoSi_2$–$Mo_5Si_3$ boundary through the lower silicide, and by the diffusion of the reacting components through the oxide layer to the boundary of the reaction where the formation of new portions of $SiO_2$ occurs [28]. The state of the silica layer is thus decisive in the progress of the reaction and the rate of oxidation essentially follows a parabolic law. However, the weight gain obtained on the RB-SiC alone observed after 160 h were less than that observed from 80 to 120 h (Fig. 9a). Why this should occur is not obvious. The weight loss of silicon which occurred after 20 h at 1400° C is not due to active oxidation but due to only volatilization of the silicon (as the melting point of 1410° C is approached). Figure 10d reveals a very rugged surface with pores, in which the silicon is volatilized.

In Fig. 10, the formation of cracks on the oxidized surface, which is completely covered with a protective layer of silica, is due partially to differences in thermal expansion and elastic properties of SiC and cristobalite [24]. In addition, the oxidized layer over the $MoSi_2$ crystals shown in Fig. 10a clearly protruded. This may be due to the $Mo_5Si_3$ which bonded together by cristobalite. However, the $Mo_5Si_3$ could be also oxidized with elevating temperature [27] (refer to the XRD result, Fig. 11). It is therefore thought that the composite is found to have developed completely smooth oxide layers by oxidation and removal of $Mo_5Si_3$, as shown in Fig. 10c. In Fig. 10a, the larger pore (arrow) in the oxide layer is not caused by CO(g) which bursts through this oxide layer, but is one of that produced during the fabrication of the composite.

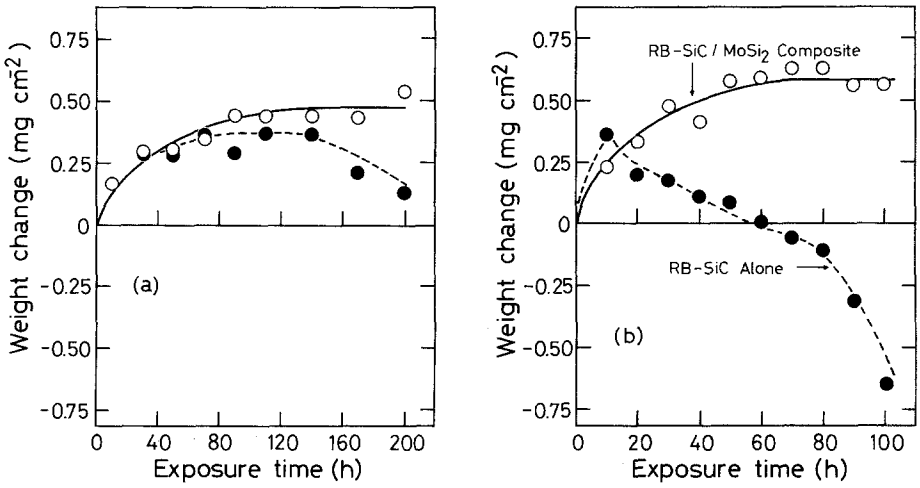


*Figure 9* Oxidation behaviour of (○) RB-SiC/17 wt % $MoSi_2$ composite and (●) RB-SiC alone, exposed in dry air at (a) 1300° C and (b) 1400° C.

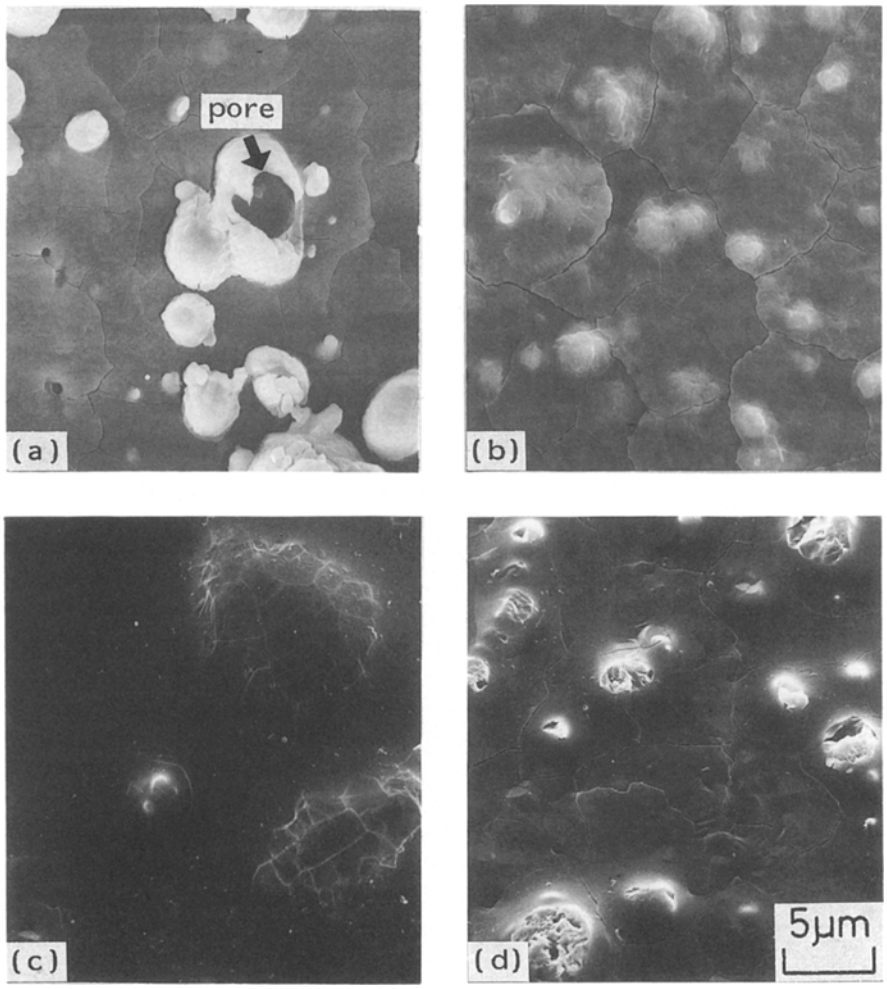


*Figure 10* SEM micrographs of surface of (a, c) RB-SiC/$MoSi_2$ composite and (b, d) RB-SiC alone involved in oxidized behaviour. (a, b) and (c, d) specimens exposed in dry air at 1300° C for 200 h and 1400° C for 100 h, respectively.

## 4. Conclusion

1. The PLS-SiC was wet by $MoSi_2$, with a contact angle of $< 90°$.

2. During infiltrating of molten $MoSi_2$ into the porous RB-SiC bulk, significant grain growth of SiC did not occur. There was good bonding between the SiC and $MoSi_2$, without significant reaction zone and microcracking caused by the thermal mismatch stresses. A thin ($\sim 2$ nm) layer at the SiC–$MoSi_2$ interface and a certain amount of strain in the SiC domain adjacent to the interface were observed.

3. The considerable difference in thermal expansion coefficient and electrical resistance was not found, between the RB-SiC alone (containing 10 wt % free silicon) and RB-SiC/17 wt % $MoSi_2$ composite.

4. At room temperature, the composite exhibited a bending strength of 410 MPa, which is low in comparison to that of RB-SiC alone (520 MPa). However,

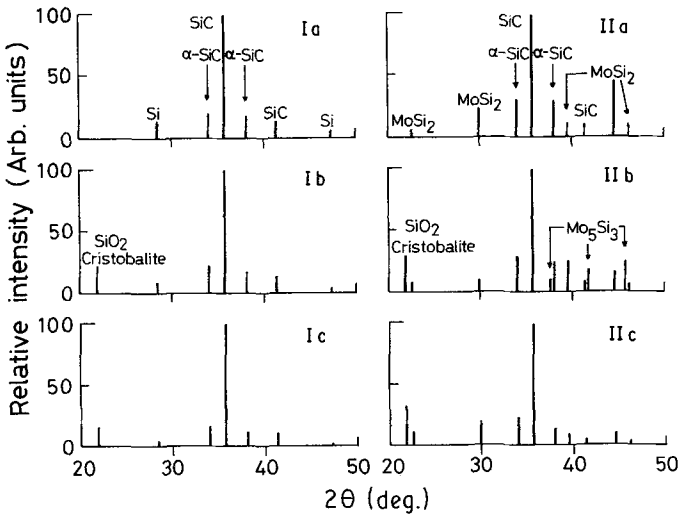


*Figure 11* Relative X-ray intensities of (Ia, Ib, Ic) RB-SiC alone and (IIa, IIb, IIc) RB-SiC/$MoSi_2$ composite (with a CuKα line source). (Ia) and (IIa) show that of as-prepared specimens. (Ib, IIb) and (Ic, IIc) show that of specimens oxidized at 1300° C for 200 h and 1400° C for 100 h, respectively.

the composite strength increased to a maximum (590 MPa) in the temperature range 1100 to 1200° C and dropped to 460 MPa between 1200 to 1400° C, after which the strength remained constant. The fracture mode in the composite was primarily transgranular and predominantly brittle at room temperature. However, there was significant evidence of the debonding at the $MoSi_2$–SiC interface at high temperature.

5. The passive oxidation of the composite in dry air in the temperature range 1300 to 1400° C was found to follow the parabolic rate law with the formation of a protective layer of cristobalite on the surface. The surface of composite oxidized at 1400° C exhibited very smooth oxide layer in comparison to that oxidized at 1300° C.

## Acknowledgement

The authors would like to acknowledge the assistance of Mr H. Suematsu in conducting TEM studies. The HREM observation was carried out using the high voltage ultra-high-vacuum-high-resolution electron microscope in Tokyo Institute of Technology.

## References

1. C. W. FORREST, P. KENNEDY and J. V. SHENNAN, "Special Ceramics 5" (British Ceramic Research Association, Stoke-on-Trent, 1972) p. 99.
2. J. N. NESS and T. F. PAGE, *J. Mater. Sci.* **21** (1986) 1377.
3. C. B. LIM and T. ISEKI, *Adv. Ceram. Mater.* **3** (1988) 590.
4. *Idem, J. Mater. Sci.* **23** (1988) 3248.
5. J. B. HUFFADINE, "Special Ceramics" (Academic Press, New York, 1960) p. 228.
6. J. B. BERKOWITZ-MATTUCK, M. ROSSETTI and D. W. LEE, *Metall. Trans.* **1** (1970) 479.
7. J. SCHLICHTING, *High Temp.-High Pressures* **10** (1978) 241.
8. N. G. SCHREWELIUS, Brit. Pat. 1023155 (1966) from Chem Abs 65 (1966) 469.
9. Bulten Kanthal AB, Ger. Pat. 2656072 (1977) from Chem Abs **88** (1978) 10832.
10. Carborundum Co., Brit. Pat. 936118 (1963) from Chem Abs **59** (1963) 13675.
11. F. D. GAC and J. J. PETROVIC, *J. Amer. Ceram. Soc.* **68** (1985) 279.
12. D. H. CARTER and G. F. HURLEY, *ibid.* **70** (1987) 79.
13. T. P. CHOW, A. J. STECKL and D. M. BROWN, *J. Appl. Phys.* **52** (1981) 6331.
14. S. PROCHAZKA, in "Silicon Carbide-1973", edited by R. C. Marshall, J. W. Faust, Jr. and C. E. Ryan (University of South Carolina Press, Columbia, 1974) p. 394.
15. J. M. GUIOT, *Silicates Ind.* **31** (1966) 457.
16. R. W. DAVIDGE and T. J. GREEN, *J. Mater. Sci.* **3** (1968) 629.
17. R. W. DAVIDGE, "Mechanical Behaviour of Ceramics" (Cambridge University Press, London, 1979) p. 80.
18. F. F. LANGE, *J. Amer. Ceram. Soc.* **56** (1973) 445.
19. F. F. LANGE, in "Fracture Mechanics of Ceramics" Vol. 2, edited by R. C. Bradt, D. P. H. Hasselman and F. F. Lange (Plenum, New York 1974) p. 599.
20. D. C. PHILLIPS, in "Handbook of Composite, Vol. 4", edited by A. Kelly and S. T. Mileiko (Elsevier, Amsterdam, 1983) p. 373.
21. D. F. CARROLL and R. E. TRESSLER, *J. Amer. Ceram. Soc.* **68** (1985) 143.
22. N. CLAUSSEN, K. L. WEISSKOPF and M. RUHLE, in "Fracture Mechanics of Ceramics, Vol. 7", edited by R. C. Bradt, A. G. Evans, D. P. H. Hasselman and F. F. Lange (Plenum, New York, 1986) p. 75.
23. W. B. HILLIG, R. L. MEHAN, C. R. MORELOCK, V. J. DECARLO and W. LASKOW, *Amer. Ceram. Soc. Bull.* **54** (1975) 1054.
24. S. C. SINGHAL, in "Ceramics for High-Performance Applications", edited by J. J. Burke, A. E. Garum and R. Nathankatzo (Brook Hill, Massachusetts, 1974) p. 533.
25. J. SCHLICHTING, *Ber. Dt. Keram. Ges.* **56** (8) (1979) 196.
26. J. SCHLICHTING and J. KRIEGESMANN, *ibid.* **56** (1979) 72.
27. U. ERNSTBERGER, H. COHRT, F. PORZ and F. THUMHLEF, *cfi/Ber. DKG.* (Ceramic forum international Berichte der Deutschen keramischen Geselschaft.) **60** (1983) 167.
28. V. I. ZMII, L. F. VERKHOROBIN, Y. N. GONTARENKO and V. P. PODTYKAN, *Vysoko Temp. Pokrytiya, Tr. Seminara, Leningrad* 1965 (pub. 1967) 209.
29. J. B. BERKOWITZ, J. T. LARSON, R. F. QUIGLEY and W. CHRISTIANSEN, *NASA Tech. Publ. Announcements* **2** (1962) 682.

*Received 3 August 1988*
*and accepted 10 January 1989*